J. Fluid Mech. (2014), *vol.* 752, *pp.* 5–21. © Cambridge University Press 2014
doi:10.1017/jfm.2014.272

Phase dynamics of freely swimming foils

Cyndee L. Finkel[1] **and Karl D. von Ellenrieder**[2,†]

[1]Department of Physics, Florida Atlantic University, Boca Raton, FL 33431, USA

[2]Department of Ocean and Mechanical Engineering, Florida Atlantic University, Dania Beach, FL 33004, USA

(Received 19 August 2013; revised 8 May 2014; accepted 12 May 2014; first published online 2 July 2014)

A two-dimensional D-shaped cylinder and heaving foil were mounted in tandem and used to simulate the main body and tail, respectively, of a natural swimmer. Thrust/drag measurements of the force on the foil and particle image velocimetry measurements of the flow downstream of the swimming system were conducted at a Reynolds number of about 10^4 in a water channel with a constant free stream current speed. Two main sets of measurements were conducted: one set with the swimming system locked at a fixed streamwise location in the water channel as the heave frequency of the foil was varied; the other set with the system freely swimming to a desired set-point position from different upstream and downstream locations. When the freely swimming system reached and maintained its set-point position, so that its swimming speed matched that of the current, the oscillation frequency of the heaving foil corresponded to a Strouhal number of 0.36. Phase portraits of the measured thrust/drag forces reveal limit cycle oscillations for all swimming cases studied, which suggests that self-regulation drives the selection of this Strouhal number. No coupling was observed between the vortices shed by the D-shaped cylinder and the self-selected frequency of the heaving foil during free swimming. An examination of the ratio of the phase-locking indices for the input heaving motion of the foil and the coupled fluidic thrust/drag response reveals that it approaches a value of 0.5 over time when the freely swimming system is released from rest and allowed to achieve steady-state cruising. The jet produced by the freely swimming foil was inclined at an angle of approximately 4° with respect to the direction of the mean flow.

Key words: biological fluid dynamics, flow–structure interactions, swimming/flying

1. Introduction

The Strouhal number corresponding to the tailbeat frequency and amplitude of a broad variety of natural swimmers has been observed to lie within the narrow range of $0.2 \leqslant St \leqslant 0.4$ (Triantafyllou, Triantafyllou & Gopalkrishnan 1991; Taylor, Nudds & Thomas 2003; Rohr & Fish 2004), where the Strouhal number is defined as

$$St = fc/U. \tag{1.1}$$

Here, f is the tailbeat frequency, c is a characteristic length scale, usually taken as the double amplitude of the motion, and U is a characteristic velocity scale, typically

† Email address for correspondence: ellenrie@fau.edu

https://doi.org/10.1017/jfm.2014.272 Published online by Cambridge University Press

taken as the steady forward speed. The question of why animals with disparate morphologies and sizes, which range from large whales to small bony fish, should swim within such a relatively narrow band of Strouhal numbers has confounded many. It has been observed that the wakes associated with thrust production by an oscillating foil are convectively unstable and tend to amplify disturbances that act at the natural vortex shedding frequency of the tail fin (Triantafyllou *et al.* 1991; Triantafyllou, Triantafyllou & Grosenbaugh 1993). Based on this observation, it has been proposed that animals may have evolved to swim in this range of Strouhal numbers to reduce the energy required for propulsion by exploiting the wake amplification for the generation of thrust. It has also been suggested that the means by which this is accomplished could be the result of a feedback process in which an animal uses a biological flow sensor, such as a lateral line system, to sense the vortices shed by its body and actively controls the motion of its tail to develop additional lift over the surface of its tail, thereby improving its overall propulsive efficiency (Triantafyllou, Triantafyllou & Yue 2000). These ideas assume a biological basis for Strouhal number selection in free swimming.

The question of what may drive the selection of Strouhal number in freely swimming animals has also been theoretically analysed by Eloy (2012). Using an extension of the elongated-body theory developed by Lighthill (1971), it is shown that the optimal Strouhal number of swimming at a constant steady-state velocity can be found as the solution to a constrained optimisation problem that minimises the mean power lost in the wake. The optimal Strouhal number is found to vary slightly as a function of the animal's geometry, as defined by the Lighthill number

$$Li = \frac{S}{h^2} C_d, \tag{1.2}$$

where S is the wetted surface area of the animal, h is the span of the tail and C_d is the animal's drag coefficient. The Lighthill number is a measure of the ratio of drag to available thrust. Assuming that animals swim at their peak propulsive efficiency, the optimal Strouhal number (and its dependence on the Lighthill number) is shown to match data from measurements on a large variety of animals fairly well (Eloy 2012). It is hypothesised that swimming animals may have evolved to optimise both the formation of a coherent wake, to take advantage of the convective instabilities identified by Triantafyllou *et al.* (1991, 1993), and their elongated-body efficiency.

At the same time, the experimental work of Vandenberghe, Zhang & Childress (2004) shows that a simple sensorless man-made system will also operate in the same narrow range of Strouhal numbers as natural swimmers do – with no intentional optimisation of the motion or geometry of the system. In their study, a flat plate is mounted from a low-friction bearing and oscillated parallel to the axis of rotation. The motion starts from a condition in which the fluid and plate are at rest. The motion of the plate undergoes a transition from a purely heaving state with no rotation to a state in which the plate is both heaving and rotating. In this latter state, the tangential speed of the tip is found to increase linearly with oscillation frequency. A reverse von Karman wake is observed behind the tip of the rotating plate, and for each of the driving frequencies studied, the Strouhal number of the motion approaches a value of 0.26.

If neither evolution nor active feedback control of foil motion is required, what physical phenomena determine the steady-state Strouhal number of a freely swimming system? Recent work has suggested that free swimming may be a passive

https://doi.org/10.1017/jfm.2014.272 Published online by Cambridge University Press

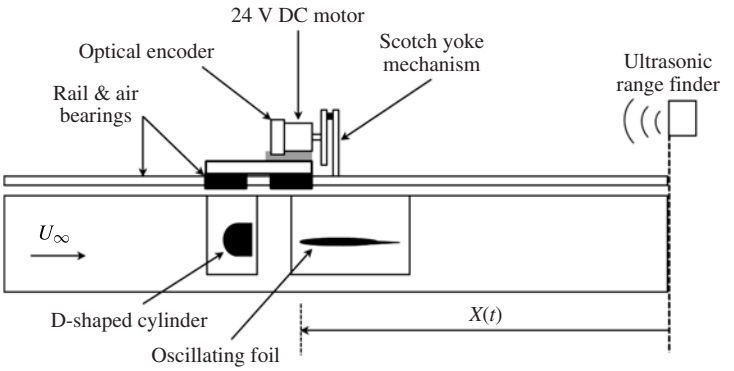


FIGURE 1. Schematic of the test section and experimental apparatus.

self-regulating process (von Ellenrieder, Parker & Soria 2008; Bandyopadhyay & Leinhos 2013). A freely swimming system may passively tune (synchronise) itself, such that the oscillation frequency of the foil matches the resonant frequency of its wake, due solely to a combination of (i) the balance of energy input by the flapping foil and energy dissipated by viscous friction/vortex shedding and (ii) coupling between the forces applied to the fluid by the oscillating foil and the corresponding lift and drag forces exerted by the fluid on the foil.

When a system reaches a self-regulated state, its phase space should display a limit cycle (Pikovsky, Rosenblum & Kurths 2003). Here, the frequency selection and phase dynamics of a freely swimming system are experimentally explored. A D-shaped cylinder and an oscillating foil are used to mimic the fore-body and tail, respectively, of a natural swimmer (figure 1). The test apparatus is designed such that its forward speed and the frequency of foil oscillation are not imposed. The swimming speed results from the balance of drag acting on the system and the thrust generated by the oscillating foil. Thus, the system self-selects the Strouhal number for steady forward motion, as a natural swimmer would.

2. Experimental apparatus and procedure

2.1. *The flow facility*

The experiments were conducted in a recirculating water channel with a 250 mm × 250 mm × 2400 mm test section. The flow facility is located on the SeaTech Campus of Florida Atlantic University and was specifically designed and constructed for particle image velocimetry (PIV) measurements. The test section is built over a 1.22 m × 2.44 m optical table and the entire structure is mounted on vibration-damping supports.

2.2. *The freely swimming system*

The freely swimming system can adjust its forward speed by altering the oscillation frequency of the foil. The system is suspended from air bearings that allow low-friction movement along the streamwise direction. A 24 V DC permanent magnet servo motor (with a 65.5:1 reduction ratio gearbox) is used to drive a Scotch yoke mechanism that oscillates the foil perpendicularly to the free stream direction in the vertical plane. A 500 count per revolution optical encoder is used to measure the

https://doi.org/10.1017/jfm.2014.272 Published online by Cambridge University Press

angular position of the motor shaft. The corresponding heave position of the foil, $h(t)$, is calculated from this measurement. Additionally, the rotational speed of the motor is determined via differentiation of the encoder measurements with respect to time. The D-shaped cylinder and foil system was found to have sufficient drag at a free stream speed of $U_\infty = 242$ mm s^{-1}, so that it is readily carried downstream by the current when deactivated, but has adequate thrust for forward swimming when operational. This free stream speed was used for all of the measurements reported here. When $U_\infty = 242$ mm s^{-1}, the foil-chord-based Reynolds number is 14.5×10^3 and the cylinder-diameter-based Reynolds number is 10.4×10^3.

2.2.1. *The oscillating foil*

The foil has a NACA0012 cross section with a chord of $c = 60.0$ mm. The foil spans the width of the tank and is suspended by two vertical acrylic plates to reduce end effects. A Scotch yoke mechanism subjects the foil to a sinusoidal heave-only motion described by

$$h(t) = h_0 \sin(2\pi ft + \phi_h), \tag{2.1}$$

where the amplitude of motion, h_0, is selected such that the double amplitude and the foil chord length are equal, f is the frequency of oscillation, ϕ_h is a phase angle and t is time. The same value of h_0 was used in all of the heaving-foil measurements reported here. Free-surface effects are expected to be negligible as the maximum Froude number of the foil, based on its minimum depth at the top dead centre of the heaving cycle, is 0.26.

2.2.2. *The D-shaped cylinder*

When in a flow, a D-shaped cylinder, with the flat part of the D facing downstream, will generate a von Kármán vortex street with a fixed wake width (Gopalkrishnan, Triantafyllou, Triantafyllou & Barrett 1994). In order to explore the possible passive synchronisation between the motion of the oscillating foil and vortex shedding from the D-shaped cylinder, the cylinder diameter was selected such that the expected natural frequency of vortex shedding from the cylinder was close in value to the expected oscillation frequency of the heaving foil for steady-state swimming – generally, the synchronisation of two or more coupled 'oscillators' can occur when they are operating at or near the same frequency (Pikovsky *et al.* 2003). The expected natural frequency of vortex shedding from the oscillating foil can be estimated as f in the definition of the Strouhal number in (1.1). Similarly, the expected shedding frequency of the D-shaped cylinder can be estimated using a modified version of (1.1), where c is replaced by the diameter of the D-shaped cylinder d. Equating the expected frequencies, taking the characteristic velocity scale to be the free stream speed U_∞, using a Strouhal number of 0.21 for the D-shaped cylinder and an intermediate value of 0.3 as the Strouhal number for the oscillating foil (see § 1), gives a diameter of $d = 42$ mm for the D-shaped cylinder. The D-shaped cylinder was constructed to the nearest fractional (Imperial) measurement during fabrication in the machine shop, giving a diameter of $d = 42.8$ mm. The resulting Strouhal number of vortex shedding by the D-shaped cylinder was experimentally measured to be $St_d = 0.22$ (see § 3.1.1).

Previous studies have shown that the thrust produced by swimming animals can be augmented by the interaction of body-shed vorticity with an oscillating tail (Gopalkrishnan *et al.* 1994; Streitlien, Triantafyllou & Triantafyllou 1996). Because of this, it has been suggested that natural swimmers might employ an active

https://doi.org/10.1017/jfm.2014.272 Published online by Cambridge University Press

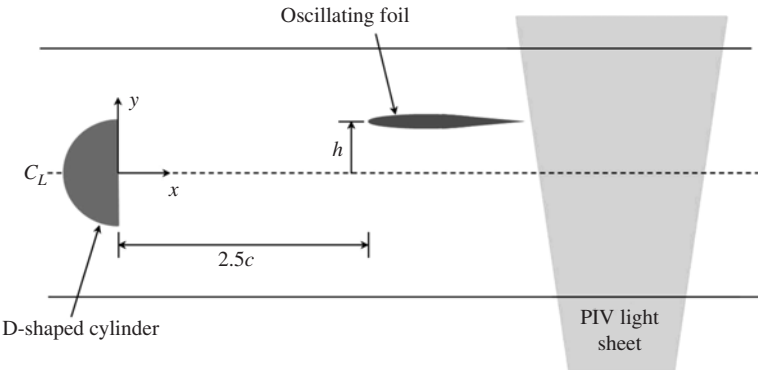


FIGURE 2. The origin of the x–y coordinate system is located on the flat downstream face of the D-shaped cylinder and along the centreline of the water tunnel. The leading edge of the oscillating foil is located a distance of $2.5c$ downstream of the rear face of the D-shaped cylinder. The light grey shaded region indicates the orientation of the PIV light sheet used for velocity measurements.

feedback control process (Triantafyllou *et al.* 2000) to appropriately synchronise the motion of the tail with oncoming vortices. Here, the intent was not to exploit tail–vortex interaction for thrust augmentation, but to explore whether or not passive synchronisation between vortex shedding and tail motion might occur. One of our hypotheses in starting out these experiments was that the coupling (synchronisation) between cylinder-shed vortices and the forces on the oscillating foil could also be the result of a passive limit cycle process. Thus, it was desirable to separate the effects of vortex–foil interaction from the effects of any interaction of the foil with the pressure field behind the cylinder. The approach taken was to position the oscillating tail far enough downstream from the D-shaped cylinder that it would be outside the cylinder's aft pressure field, but close enough that there would still be interaction between the oscillating foil and the vortices shed by the cylinder.

A two-dimensional control volume analysis was used to determine that a separation distance of 2.5 foil chord lengths would be sufficient (figure 2). The flow was assumed to be two dimensional because the aspect ratio of the D-shaped cylinder is 5.7 (cylinder span l to diameter ratio) and the cylinder is suspended from acrylic endplates to reduce three-dimensional end effects. As shown in many texts, e.g. Kundu & Cohen (2004), an expression for the conservation of momentum of the flow about the cylinder can be written as

$$\int_V \frac{\partial}{\partial t}(\rho \boldsymbol{u})\mathrm{d}V + \int_S (\rho \boldsymbol{u}\boldsymbol{u}) \cdot \mathrm{d}\boldsymbol{S} = \int_S (-p\boldsymbol{I} + \boldsymbol{\tau}) \cdot \mathrm{d}\boldsymbol{S} + \int_V \rho \boldsymbol{f}\,\mathrm{d}V, \tag{2.2}$$

where ρ is the density of the fluid, $\boldsymbol{u}$ is the velocity, $\boldsymbol{\tau}$ is the viscous stress tensor, V is a control volume that surrounds the cylinder and is bounded by a control surface S, $\boldsymbol{I}$ is the identity matrix and $\boldsymbol{f}$ is a vector of the body forces acting in V (e.g. gravity). Although V surrounds the D-shaped cylinder, it does not include the volume of the cylinder. As only the forces acting on the D-shaped cylinder are sought, the heaving foil is omitted from the analysis. Here, the steady mean force acting on V is examined so that the volume integral on the left-hand side of (2.2) can be neglected. The control surface S is comprised of the subsurfaces AB, BC, CD, AD

https://doi.org/10.1017/jfm.2014.272 Published online by Cambridge University Press

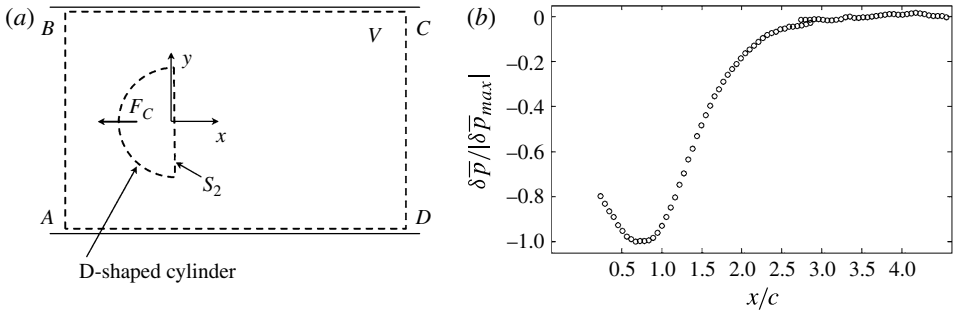


FIGURE 3. (*a*) Sketch of the control volume V and the corresponding surface S (dashed lines) used for the determination of the drag F_C on the D-shaped cylinder in (2.2). (*b*) The normalised integrated pressure variation $\delta\bar{p}/|\delta\bar{p}_{max}|$, plotted as a function of position downstream from the D-shaped cylinder when $U_\infty = 242$ mm s^{-1}.

and S_2 (figure 3*a*). The velocity normal to the surfaces BC, AD and S_2 is zero, so the surface integral over S on the left-hand side of (2.2) reduces to an integral over the surfaces of AB and CD. If we take only the streamwise components of (2.2), we obtain

$$\int_{CD} \rho u^2 \mathrm{d}S - \int_{AB} \rho U_\infty^2 \mathrm{d}S = \left[\int_{AB+CD} (-p\boldsymbol{I} + \boldsymbol{\tau}) \cdot \mathrm{d}\boldsymbol{S} + \int_{S_2} (-p\boldsymbol{I} + \boldsymbol{\tau}) \cdot \mathrm{d}\boldsymbol{S} \right] \cdot \boldsymbol{e}_x, \quad (2.3)$$

where $\boldsymbol{e}_x$ is the unit vector in the x direction. The effect of any boundary layers, which may be present on the bottom and side walls of V, is ignored. The rightmost integral term in (2.3) is the drag on the D-shaped cylinder F_C that acts on the control volume V. The surface AB is taken far upstream of the cylinder where the velocity is uniform and there is no shear stress. As the wake behind the cylinder is symmetric about x, the integral of the shear stress at surface CD also vanishes. Applying conservation of mass in V and rearranging the terms in (2.3) gives

$$\int_{CD} \rho U_\infty (U_\infty - u) l \mathrm{d}y - F_C = -\int_{CD} (p - p_\infty) l \mathrm{d}y \equiv \delta\bar{p}, \quad (2.4)$$

where p_∞ is the free stream pressure. When the surface CD is located far downstream where the local pressure is equivalent to p_∞, the pressure integral in (2.4) vanishes and the integral of the momentum change across V is equal to F_C. Using mean PIV measurements (§ 2.3.2) of the flow downstream of the D-shaped cylinder (without the foil in the flow), the streamwise velocity is integrated as in (2.4) to estimate the integrated pressure variation across V, $\delta\bar{p}$. By plotting $\delta\bar{p}$ normalised by the magnitude of its maximum value $|\delta\bar{p}_{max}|$, it can be seen that $\delta\bar{p} = 0.07|\delta\bar{p}_{max}|$ at a downstream position of $x = 2.5c$. The integrated pressure variation at this location was taken to be small enough that the leading edge of the foil could be positioned there without significant effects from the D-shaped cylinder's aft pressure field.

2.2.3. *Control for steady-state cruising*

A single-input/single-output closed-loop proportional-integral (PI) controller automatically regulates the horizontal position of the system in the test section of the water channel. The controller utilises an ultrasonic rangefinder for position

https://doi.org/10.1017/jfm.2014.272 Published online by Cambridge University Press

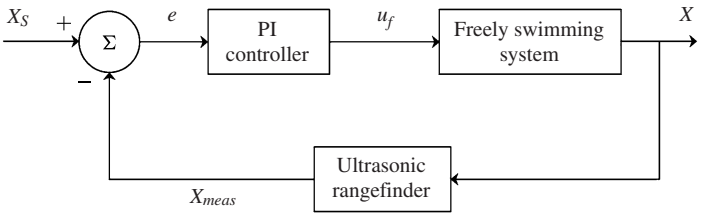


FIGURE 4. The closed-loop control system.

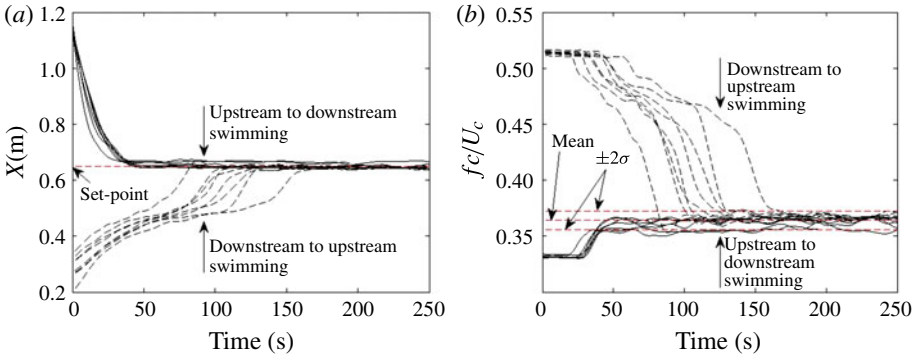


FIGURE 5. (Colour online) (*a*) X-location versus time for multiple runs that start from different initial positions. (*b*) The corresponding Strouhal values of the system. The mean value found after it reaches steady state, t_{ss}, is indicated by a horizontal dashed line ($U_c = 295$ mm s^{-1} at steady state, see § 2.3.2). Downstream to upstream swimming is indicated by dashed lines; upstream to downstream swimming is indicated by solid lines.

feedback and adjusts the oscillation frequency of the foil to drive the system toward a desired X-location set-point (figure 1).

The control law is given by the equation

$$u_f(t) = K_P\, e(t) + K_I \int_0^t e(\tau)\mathrm{d}\tau, \tag{2.5}$$

where e is the error between X_d, the desired set-point position, and X_{meas}, the measured position of the swimming system, so that $e = (X_d - X_{meas})$ – see figure 4. The output of the controller, u_f, is a voltage input to the DC motor, which drives the frequency of the oscillating foil. The proportional gain K_P and the integral gain K_I, which are constant, were determined using the Ziegler–Nichols tuning method (Franklin, Powell & Emami-Naeini 1994).

Data were collected for multiple upstream and downstream swims to a set-point of $X = 65$ cm (figure 5*a*). Steady-state cruising is considered to have been achieved when the controller maintains the location of the freely swimming system at its set-point in a constant free stream current and the speed of any deviations about the set-point remains small, $|\mathrm{d}X/\mathrm{d}t| < 1$ mm s^{-1} (figure 6*a*). During cruising, the thrust produced by the oscillating foil, F_T, will match the total drag acting on the system, F_D (both the D-shaped cylinder and the foil). The time series of the swimming system can be separated into two regions of interest, the transition region, which occurs during acceleration/deceleration, and the steady-state region, where

https://doi.org/10.1017/jfm.2014.272 Published online by Cambridge University Press

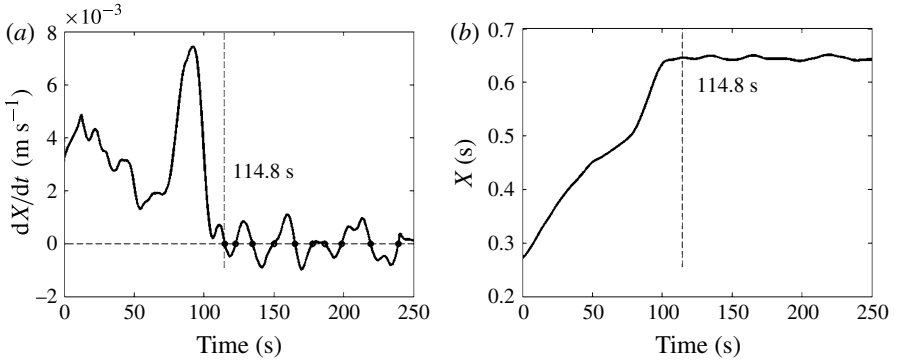


FIGURE 6. (*a*) Example of the transition time to steady state found with $|\mathrm{d}X/\mathrm{d}t| \to 0$. Each zero-speed crossing is marked by a circle. (*b*) The corresponding X-location of the system. The time at which steady state is achieved, t_{ss}, is indicated by a vertical dashed line ($U_c = 295$ mm s^{-1} at steady state, see § 2.3.2).

cruising occurs at the set-point. When the system starts downstream and must swim upstream to reach the set-point, the streamwise force on the foil transitions from $F_T > F_D$ to $F_T = F_D$. Conversely, when the system starts upstream and gets carried downstream by the current, the streamwise force on the foil transitions from $F_D > F_T$ to $F_T = F_D$. For a given starting distance from the set-point, the transition times for runs in which the initial position was located upstream were shorter than those in which the initial position was downstream. In general, the unsteady response of a closed-loop system (rise time, settling time, overshoot, etc.) is affected by the values of the controller gains and the dynamics of the feedback sensors/actuators selected. However, as evidenced by the fact that the steady-state phase dynamics of both backward and forward swimming shown in § 3.2 are essentially the same, it is likely that the steady-state phase dynamics of the system are not significantly affected by the control parameters.

2.3. *Thrust/drag and flow measurements*

A computer-controlled data acquisition system was used for both measurement and control. A digital to analogue output module with 16 bit resolution and an update rate of 100×10^3 Hz is connected to a motor driver to control the oscillation frequency of the foil. Two 5 V TTL bidirectional high speed digital input/output modules are employed: one module is interfaced with the ultrasonic range finder; the other is used to record the encoder frequency.

2.3.1. *Thrust/drag measurements*

The thrust/drag acting on the oscillating foil is measured using a force flexure constructed from a thin strip of aluminium. Four linear strain gauges are mounted on the flexure in a Wheatstone bridge configuration that self-compensates for temperature and torsion. Since the strain gauges are used in humid conditions with possible splashing, they are coated with a thin layer of wax. During static calibration, a linear relation between the output voltage and the force acting at the end of the force flexure was determined. The force data are sampled at a rate of 20 Hz using a 16 bit analogue-to-digital converter.

https://doi.org/10.1017/jfm.2014.272 Published online by Cambridge University Press

In order to find the phase angle from a time series, it is necessary to verify that the system is oscillatory. This is accomplished when significant peaks can be identified in the power spectrum of the force output, F_T. When the system is locked on the rails, the power spectrum can be evaluated using the fast Fourier transform (FFT) method. However, since the freely swimming system measurements are non-stationary the use of FFTs does not give an accurate representation of the power spectrum. Thus, the forces measured during free swimming are evaluated using the short-time Fourier transform method. The forces were found to be oscillatory in all of the locked on rails and freely swimming cases studied (Finkel 2013).

2.3.2. *Flow measurements*

Planar two-dimensional PIV is used to measure the mean $\boldsymbol{U} = (U, V, W)$ and instantaneous $\boldsymbol{u} = (u, v, w)$ velocity fields, as well as, the vortex shedding frequencies of the D-shaped cylinder and oscillating foil. Here, the coordinate system for PIV analysis is located immediately at the downstream (trailing) edge of the object such that $x = 0$. The mean centreline of the foil and D-shaped cylinder are located at $y = 0$, and the plane of the laser sheet is at $z = 0$. In this work, the mean flow in the streamwise direction, $U(x, y)$, is found by averaging the velocity at each $(x, y, 0)$ point over time. All mean data presented were measured using 900 consecutive PIV image pairs.

The PIV light sheet is generated using a dual-cavity high-energy pulsed Nd:YAG laser. The PIV images are acquired using a one megapixel digital CCD camera to capture the light scattered at 90° from the laser light sheet. The flow was seeded with 11 μm spherical particles. Post-processing of the vectors was carried out using a central difference image correction (CDIC) deformation algorithm combined with the Hart correlation method with an interrogation region of 32 pixel $\times$ 32 pixel with 75 % overlap. The vector fields were validated using standard velocity range criteria and a 3×3 local median filter. Missing vectors were interpolated using a 3×3 local mean technique.

Since the frontal area of the cylinder is 17.9 % of the working cross-sectional area of the water channel, the free stream velocity is corrected for blockage effects using the expression

$$U_c = U_\infty \frac{H}{H - d} \tag{2.6}$$

(Bishop & Hassan 1964; Liao, Dong & Lu 2004; Beal, Hover, Triantafyllou, Liao & Lauder 2006; Przybilla, Kunze, Rudert, Bleckmann & Brücker 2010). Here, U_c is the corrected velocity and $H = 24$ cm is the height of the water in the channel.

3. Results and discussion

3.1. *Frequency selection in swimming*

3.1.1. *D-shaped cylinder*

The vortex shedding frequency of the D-shaped cylinder was determined by identifying peaks in the power spectrum of v measured at the location $(x, y, z) = (3d, 0, 0)$. These measurements were conducted without the foil present in the test section. When the cylinder diameter d and free stream speed U_∞ were used to determine the Strouhal number St_d, a dominant vortex shedding frequency corresponding to $St_d = fd/U_\infty = 0.22$ was found, which agrees with the value reported by Gopalkrishnan *et al.* (1994). If, as will be the case for the remainder of the results

https://doi.org/10.1017/jfm.2014.272 Published online by Cambridge University Press

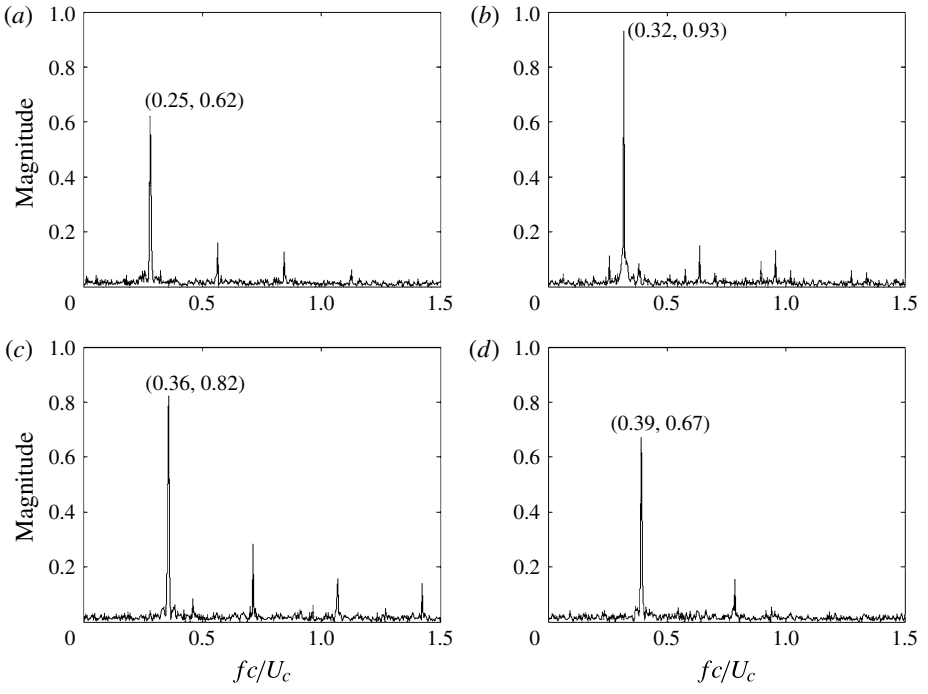


FIGURE 7. Power spectra of v in the wake when the system is locked on the rails for Strouhal numbers of (*a*) 0.28, (*b*) 0.32, (*c*) 0.36 and (*d*) 0.39 ($U_c = 295$ mm s^{-1}).

presented below, the foil chord length c and the blockage-corrected free stream speed U_c are taken as the characteristic length scale and velocity scale, respectively, the Strouhal number of vortex shedding corresponds to $St = fc/U_c = 0.25$.

3.1.2. *Oscillating foil*

Two sets of experiments were conducted to explore the dominant frequencies of the flow structures shed into the wake of the swimming system when both the D-shaped cylinder and the foil were mounted. In the first set of experiments, the swimming system was locked in place on the rails at a fixed X-position. The oscillation frequency of the foil f was varied. In the second set of experiments, the freely swimming system was released from multiple upstream and downstream positions and permitted to achieve steady-state free swimming at the set-point.

Figures 7*a–d* show the power spectra of v for various values of driving frequency $St = fc/U_c$ when the swimming system is locked on the rails. The largest peak in each spectrum corresponds to the driving frequency of the foil. The most energetic structures were not observed at the maximum driving frequency, but at a driving frequency of $St = 0.32$ (figure 7*b*). An additional peak at about $St = 0.25$ appears at this driving frequency, but not at the others. It is likely that this additional peak is generated by vortex shedding from the D-shaped cylinder (see § 3.1.1 above), which suggests that the vortices shed by the oscillating foil at other driving frequencies may suppress or break up the vortices shed by the cylinder. The higher-order harmonics of the foil oscillation frequency appear to be largest at a driving frequency of $St = 0.36$, which is the steady-state Strouhal number measured for the freely swimming system. As mentioned in § 1, Triantafyllou *et al.* (1991) and Triantafyllou *et al.* (1993) have

https://doi.org/10.1017/jfm.2014.272 Published online by Cambridge University Press

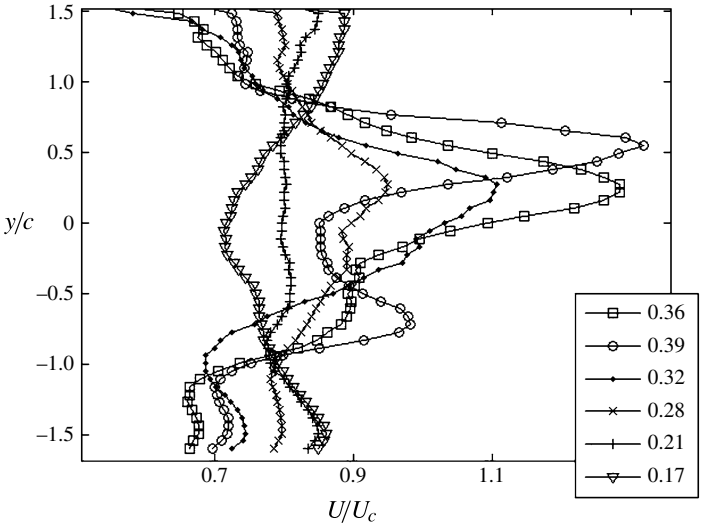


FIGURE 8. Average velocity profiles in the wake, taken at a streamwise distance of one chord length downstream from the trailing edge of the oscillating foil, when the system is locked on the rails ($U_c = 295$ mm s^{-1}). The numbers in the legend indicate the Strouhal numbers corresponding to the driving frequencies of the foil.

shown that swimming wakes associated with thrust are convectively unstable and tend to amplify disturbances that act near the Strouhal number of natural vortex shedding. Thus, the freely swimming system may be tuning itself so that the frequency of foil oscillation corresponds to the natural shedding frequency of the wake.

An examination of the average velocity in the wake was first carried out with the system locked on its rails and oscillated at different heave frequencies (figure 8). As the Strouhal number was increased, the wake was observed to transition from a drag-producing wake, to a thrust-producing wake, to an inclined jet (Jones, Dohring & Platzer 1988; von Ellenrieder & Pothos 2008; Ren, Hu, Liu & Wu 2013) and then to a double jet (at $St = 0.39$).

During steady-state free swimming, the mean velocity profiles show a deflected wake that is inclined at an angle of approximately 4° to the streamwise direction at a driving frequency of $St = 0.36$ (figure 9*a*). The deflected wake is similar to those reported in both experimental and numerical studies at this Strouhal number for oscillating foil systems mounted at a fixed streamwise location (Heathcote & Gursul 2007; von Ellenrieder & Pothos 2008; Godoy-Diana, Aider & Wesfreid 2008; Godoy-Diana, Marais, Aider & Wesfreid 2009).

In every free swimming case studied, the oscillation frequency of the flapping foil asymptotically approached a value corresponding to $St = 0.36$ over time as the system began to achieve steady-state cruising (figure 9*b*). Thus, self-regulation in cruising appears to stay within a bounded region of St with no external flow sensory input. However, the heave frequency did not lock on to the shedding frequency of the cylinder. Instead, the frequency corresponded to the imposed heave motion of the foil.

Previous studies have suggested that the St selected in natural swimming may be the result of flow sensing of body-shed vortices by a lateral line system and active tail control to exploit the presence of those vortices for enhanced propulsion

https://doi.org/10.1017/jfm.2014.272 Published online by Cambridge University Press

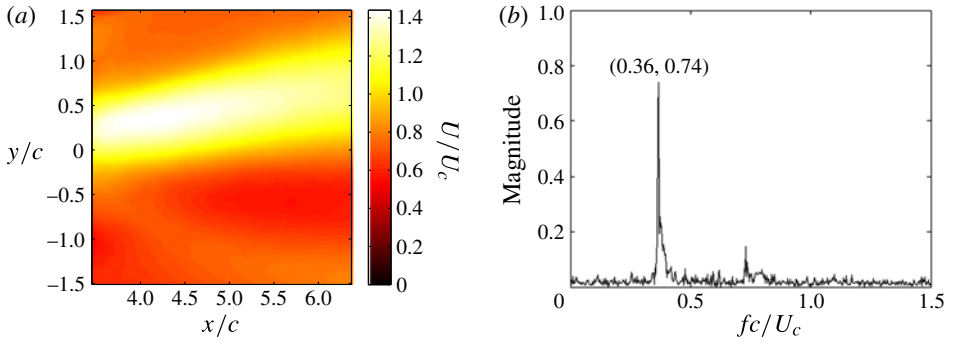


FIGURE 9. (Colour online) (*a*) Average streamwise speed U normalised by $U_c = 295$ mm s^{-1} in the flow behind the freely swimming system after it has reached the set-point from downstream. (*b*) Power spectrum of $v(t)$ in the wake after the system swims upstream.

(Triantafyllou *et al.* 2000). Here, the frequency of tail oscillation and vortex shedding by the D-shaped cylinder are uncoupled, suggesting that no flow-sensing feedback is necessary in these experiments for frequency selection. von Ellenrieder *et al.* (2008) suggested that the selection of tailbeat frequency in natural swimming may correspond to a passive limit cycle process representing the synchronisation of multiple coupled oscillators: body-shed vortices, the motion of the tail and tail-shed vortices. While reducing the separation distance between the D-shaped cylinder and the oscillating foil so that the foil operates within the time-varying pressure field of the D-shaped cylinder (see § 2.2.2) might more strongly couple vortex shedding by the cylinder and the oscillating foil, such coupling was not observed and does not appear to be generally necessary for the selection of St in free swimming. Rather, St selection appears to be the consequence of mode locking between the foil's motion input and fluidic response via vortex shedding.

3.2. *Dynamical systems analysis*

The method of analytic signals is applied to determine the phase space of the system by converting the time series thrust/drag and heave position measurements into complex functions of time (Rosenblum, Pikovsky & Kurths 1996; Pikovsky, Rosenblum, Osipov & Kurths 1997). It should be noted that, in contrast to plotting the phase plane of a signal as the signal versus its time derivative (Strogatz 1994), this method is often used to analyse experimental data as it permits one to avoid the amplification of signal noise that can result when taking the time derivative of an experimental measurement (Boashash 1992; Rosenblum, Pikovsky, Kurths, Schäfer & Tass 2001; Pikovsky *et al.* 2003). A Hilbert transform is used to generate a phase quadrature component that serves as the imaginary part of the time-varying signal $F(t)$ using the Cauchy principal value (PV)

$$F^* = \pi^{-1} PV \int_{-\infty}^{\infty} \frac{F(\tau)}{t-\tau} \mathrm{d}\tau. \tag{3.1}$$

The complex equation generated from the signal $F(t)$ is

$$\psi(t) = F(t) + \mathrm{i}F^*(t) = a(t)\exp^{\mathrm{i}\phi(t)}, \tag{3.2}$$

https://doi.org/10.1017/jfm.2014.272 Published online by Cambridge University Press

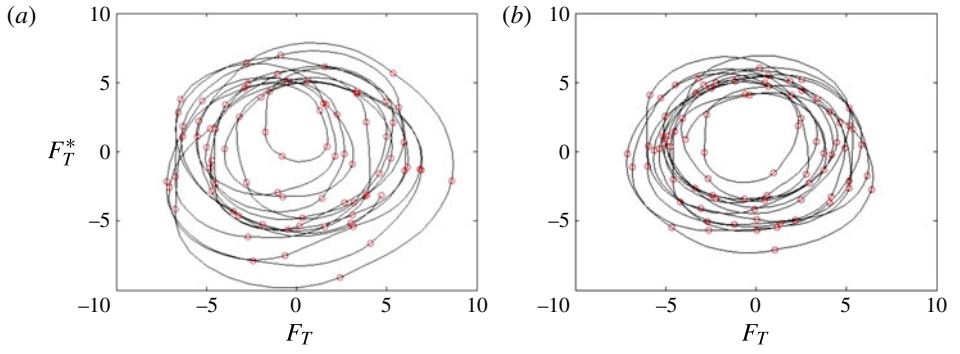


FIGURE 10. (Colour online) The phase space constructed from F_T during steady forward swimming after the system has reached the set-point from (*a*) downstream and (*b*) upstream. Here, $U_c = 295$ mm s^{-1} at steady state.

where $a(t)$ and $\phi(t)$ are the instantaneous amplitude and phase, respectively. The three-dimensional phase space representation has state parameters (F, F^*, ϕ).

3.2.1. *Phase portrait*

The phase portrait of F_T was examined when the system was locked in a fixed streamwise X-position, as well as when it was freely swimming. When locked on the rails, F_T demonstrates a limit cycle trajectory at each of the imposed heave frequencies tested, which correspond to $St = fc/U_c = \{0.13, 0.17, 0.21, 0.28, 0.32, 0.36, 0.39\}$ (Finkel 2013). Likewise, at steady-state cruising, the phase spaces of the swimming data sets show a limit cycle structure (figures 10*a,b*), regardless of the initial position of the swimming system. Thus, the limit cycle structure appears to exist for each of the runs performed, suggesting that the coupling between the heaving motion of the foil and the force response of the fluid is a self-regulated process for each condition tested (Bandyopadhyay & Leinhos 2013). As shown in the following section (§ 3.2.2), the main difference between heaving foils operating near the $F_T = F_D$ condition and those operating away from it is that the ratio of the instantaneous phase angles of the input heave position and the output fluidic force always approaches 1/2. The value may be indicative of two vortices being shed per foil oscillation cycle – a condition associated with high propulsive efficiency (Anderson, Streitlien, Barrett & Triantafyllou 1998).

3.2.2. *Phase locking*

The input heaving motion of the foil and the resulting fluidic thrust/drag are synchronised (mode-locked) when the phase difference between the measured signals is bounded. The instantaneous phase of each measurement is calculated using (3.2), where the phase angle of the signal $F(t)$ is

$$\phi(t) = \arctan\left[\frac{F^*(t)}{F(t)}\right]. \tag{3.3}$$

For the oscillating foil, m:n phase locking occurs when the phase of $F_T(t)$, which is denoted as ϕ_F, and the phase of $h(t)$, which is represented as ϕ_h, have the relationship

$$\Delta\phi_{m,n} = |m\phi_F(t) - n\phi_h(t)| < \text{constant}. \tag{3.4}$$

https://doi.org/10.1017/jfm.2014.272 Published online by Cambridge University Press

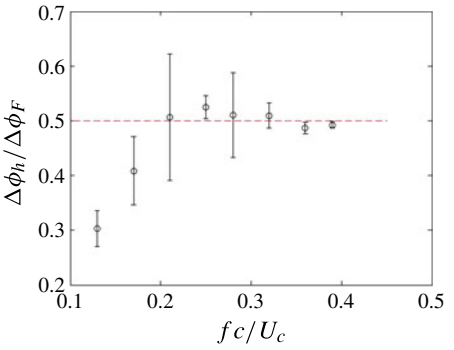


FIGURE 11. (Colour online) The m:n locking ratio for each St value tested when the system is fixed on the rails – a convergence to $m/n = 0.5$ as $F_T \to F_D$ can be seen. The circles represent the mean locking ratio for the data sets analysed and the error bars indicate the corresponding standard deviation ($U_c = 295$ mm s^{-1}).

These phase-locking parameters are determined by examining the simplest condition of (3.4), which is equivalent to frequency locking, $m\Omega_F = n\Omega_h$. Thus, the ratio

$$\frac{m}{n} = \frac{\Delta\phi_h}{\Delta\phi_F} = \frac{\phi_h(t+\Delta t) - \phi_h(t)}{\phi_F(t+\Delta t) - \phi_F(t)} \tag{3.5}$$

gives the locking value, where Δt is the time between measurements. A sliding window 30 s in length and with 75 % overlap was used to explore how the locking ratio evolves in time. The sliding window was used to break the time series (3.5) into shorter time segments; a local linear fit to the m/n data in each time segment was used to determine the locking ratio.

This technique was first applied to the data sets for the system mounted in a fixed X-position. Figure 11 shows the locking ratio measured for each St value. The phase-locking ratio converges to $m/n = 0.5$ as St is increased.

This was repeated when the system was freely swimming to determine how the ratio varies as the steady-state cruising condition is approached in time. Figure 12 shows that convergence to $m/n = 0.5$ also occurs. The m:n locking during steady state was calculated for each free swimming run and found to be within 3 % of $m/n = 0.5$.

The classical theories of fish swimming developed by Lighthill (1971) and Wu (1961) predict that the frequency of the transverse undulation of a freely swimming waving plate (representing the body of a fish) will be half of the frequency of the thrust generated. The experimental force measurements of Read, Hover & Triantafyllou (2003) also reveal that the frequency of the lift signal generated by a heaving and pitching foil at $St = 0.4$ will be half of the frequency of the thrust generated. Thus, frequency locking with an $m/n = 0.5$ ratio is also apparent in these previous studies of steady-state systems. The results presented here complement and extend these previous studies by showing how the phase-locking ratio evolves over time as a freely swimming system is released from rest and gradually reaches an equilibrium condition when thrust and drag are balanced.

4. Concluding remarks

One of the key findings of this work is that a freely swimming system passively selects the Strouhal number at which it swims, without the need for feedback from

https://doi.org/10.1017/jfm.2014.272 Published online by Cambridge University Press

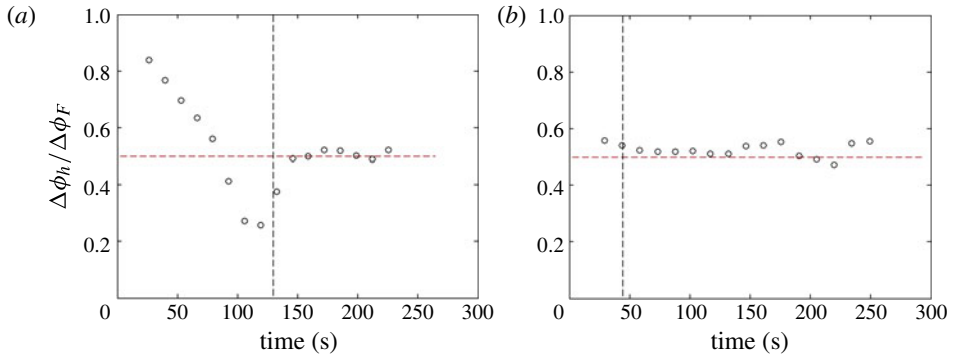


FIGURE 12. (Colour online) The m:n locking ratio for (*a*) forward and (*b*) backward swimming. The vertical dashed lines correspond to t_{ss} and the horizontal dashed lines indicate $m/n = 0.5$. The circles show the mean locking ratio during each 30 s sliding-window time segment ($U_c = 295$ mm s^{-1} at steady state).

any flow sensors. When a foil is oscillated at a given frequency, the system's forward speed increases/decreases until thrust and drag balance – at that point the specific Strouhal number of motion has been passively selected and always approaches the same value (for a given system geometry). Here, it is asserted that the system possesses all of the key characteristics of a limit cycle oscillator (Pikovsky *et al.* 2003): there is a constant (internal) source of energy input, a source of energy dissipation and the existence of weak coupling between the forced motion of the foil and the resulting fluidic response. Identification of the presence of a limit cycle is significant because it demonstrates the bounded stability of the coupled fluid–foil system in always approaching the same steady-state equilibrium condition for a given forcing input, system geometry and flow speed. As discussed in von Ellenrieder *et al.* (2008), a consequence of this is that only relatively simple sensory and control hardware may be required to regulate the steady forward motion of man-made biomimetically propelled vehicles. Sensory feedback may be more important for manoeuvring/acceleration. Additionally, the response of freely swimming systems to current-induced speed fluctuations could be largely passive. However, additional research is necessary to extend the possible implications of the results obtained using the man-made system studied here to sensing in biological systems.

It has not been shown here that the Strouhal number passively selected in free swimming is 'optimal', e.g. in a sense that it maximises the system's propulsive efficiency or minimises the energy lost to the wake. However, the Strouhal number found in the present study is close in value to those reported as providing optimal propulsive efficiency in other work (Anderson *et al.* 1998; Triantafyllou *et al.* 2000; Read *et al.* 2003; Eloy 2012). As pointed out by Bandyopadhyay & Leinhos (2013), limit cycle oscillators tend to self-regulate to a condition that minimises energy loss. An interesting avenue of future work would be to directly measure the propulsive efficiency of a freely swimming system and explore how it evolves in time as the system reaches steady-state cruising.

As the main objective of the work presented here was to explore the phase and limit cycle dynamics of free swimming, foil chord length, cylinder diameter and cylinder–foil spacing were not varied during the experiments. Thus, the scope of the present work does not enable the characterisation of how any system invariants

https://doi.org/10.1017/jfm.2014.272 Published online by Cambridge University Press

determined from combinations of these experimental parameters might affect the value of the Strouhal number. Eloy (2012) identified some dependence of the Strouhal number on the Lighthill number. As variations in system geometry will affect each of the parameters that comprise the Lighthill number (1.2), there may be corresponding variations in the Strouhal number. The use of a robotic mechanism, such as the one developed here, to explore the dependence of Strouhal number selection on system geometry would be a very interesting avenue of research to pursue, especially as a means of further studying/validating the relationship between the Lighthill and Strouhal numbers proposed by Eloy (2012).

Lastly, no coupling was observed between the vortices shed by the D-shaped cylinder and the frequency of the heaving foil, as might be expected in natural swimmers (Triantafyllou *et al.* 2000). If reduction of the separation distance between the foil and the D-shaped cylinder leads to coupling, a study of the influence of that coupling on the passive selection of foil oscillation frequency could be of benefit to an understanding of the energetics of natural swimming.

Acknowledgements

The authors would like thank Professors K. Sorge and A. Fuchs for their helpful insights on nonlinear dynamics, as well as Mr T. Furfaro for his assistance with the experimental apparatus and instrumentation. The first author gratefully acknowledges the sponsorship of the Link Foundation Ocean Engineering & Instrumentation PhD Fellowship Program. This work was also partially supported by the US Air Force Office of Scientific Research (Grant FA9550-07-1-0588).

REFERENCES

ANDERSON, J. M., STREITLIEN, K., BARRETT, D. S. & TRIANTAFYLLOU, M. S. 1998 Oscillating foils of high propulsive efficiency. *J. Fluid Mech.* **360**, 41–72.

BANDYOPADHYAY, P. R. & LEINHOS, H. A. 2013 Propulsion efficiency of bodies appended with multiple flapping fins: when more is less. *Phys. Fluids* **25**, 041902.

BEAL, D. N., HOVER, F. S., TRIANTAFYLLOU, M. S., LIAO, J. C. & LAUDER, G. V. 2006 Passive propulsion in vortex wakes. *J. Fluid Mech.* **549**, 385–402.

BISHOP, R. E. D. & HASSAN, A. Y. 1964 The lift and drag forces on a circular cylinder in a flowing fluid. *Proc. R. Soc. Lond.* A 7 **277** (1368), 32–50.

BOASHASH, B. 1992 Estimating and interpreting the instantaneous frequency of a signal – part 1: fundamentals. *Proc. IEEE* **80** (4), 520–538.

VON ELLENRIEDER, K. D., PARKER, K. & SORIA, J. 2008 Fluid mechanics of flapping wings. *Exp. Therm. Fluid Sci.* **32** (8), 1578–1589.

VON ELLENRIEDER, K. D. & POTHOS, S. 2008 PIV measurements of the asymmetric wake of a two dimensional heaving hydrofoil. *Exp. Fluids* **44**, 733–745.

ELOY, C. 2012 Optimal Strouhal number for swimming animals. *J. Fluids Struct.* **30**, 205–218.

FINKEL, C. L. 2013 Synchronization and phase dynamics of oscillating foils. PhD thesis, Florida Atlantic University, Boca Raton, FL, USA.

FRANKLIN, G. F., POWELL, J. D. & EMAMI-NAEINI, A. 1994 *Feedback Control of Dynamic Systems*, 3rd edn. Addison-Wesley.

GODOY-DIANA, R., AIDER, J.-L. & WESFREID, J. E. 2008 Transitions in the wake of a flapping foil. *Phys. Rev.* E **77** (1), 016308.

GODOY-DIANA, R., MARAIS, C., AIDER, J. L. & WESFREID, J. E. 2009 A model for the symmetry breaking of the reverse Bérnard–von Kármán vortex street produced by a flapping foil. *J. Fluid Mech.* **622**, 23–32.

https://doi.org/10.1017/jfm.2014.272 Published online by Cambridge University Press

GOPALKRISHNAN, R., TRIANTAFYLLOU, M. S., TRIANTAFYLLOU, G. S. & BARRETT, D. 1994 Active vorticity control in a shear flow using a flapping foil. *J. Fluid Mech.* **274**, 1–21.

HEATHCOTE, S. & GURSUL, I. 2007 Jet switching phenomenon for a periodically plunging airfoil. *Phys. Fluids* **19** (2), 027104.

JONES, K. D., DOHRING, C. M. & PLATZER, M. P. 1988 Experimental and computational investigation of the Knoller–Betz effect. *AIAA J.* **36** (7), 1240–1246.

KUNDU, P. K. & COHEN, I. M. 2004 *Fluid Mechanics*, 3rd edn. Elsevier Inc.

LIAO, Q., DONG, G. J. & LU, X. Y. 2004 Vortex formation and force characteristics of a foil in the wake of a circular cylinder. *J. Fluid Struct.* **19**, 491–510.

LIGHTHILL, M. J. 1971 Large-amplitude elongated-body theory of fish locomotion. *Proc. R. Soc. Lond.* B **179** (1055), 125–138.

PIKOVSKY, A., ROSENBLUM, M. & KURTHS, J. 2003 *Synchronization: a Universal Concept in Nonlinear Sciences*. vol. 12. Cambridge University Press.

PIKOVSKY, A. S., ROSENBLUM, M. G., OSIPOV, G. V. & KURTHS, J. 1997 Phase synchronization of chaotic oscillators by external driving. *Physica* D **104**, 219–238.

PRZYBILLA, A., KUNZE, S., RUDERT, A., BLECKMANN, H. & BRÜCKER, C. 2010 Entraining in trout: a behavioural and hydrodynamic analysis. *J. Expl Biol.* **213**, 2976–2986.

READ, D. A., HOVER, F. S. & TRIANTAFYLLOU, M. S. 2003 Forces on oscillating foils for propulsion and maneuvering. *J. Fluid Struct.* **17**, 163–183.

REN, WEI, HU, HUI, LIU, HONG & WU, JAMES C 2013 An experimental investigation on the asymmetric wake formation of an oscillating airfoil. *AIAA paper* 2013-0794.

ROHR, J. J. & FISH, F. E. 2004 Strouhal numbers and optimization of swimming by odontocete cetaceans. *J. Expl Biol.* **207**, 1633–1642.

ROSENBLUM, M., PIKOVSKY, A., KURTHS, J., SCHÄFER, C. & TASS, P. A. 2001 Phase synchronization: from theory to data analysis. Handbook of Biological Physics, vol. 4. Elsevier Science.

ROSENBLUM, M. G., PIKOVSKY, A. S. & KURTHS, J. 1996 Phase synchronization of chaotic oscillators. *Phys. Rev. Lett.* **76** (11), 1804–1807.

STREITLIEN, K., TRIANTAFYLLOU, G. S. & TRIANTAFYLLOU, M. S 1996 Efficient foil propulsion through vortex control. *AIAA J.* **34** (11), 2315–2319.

STROGATZ, S. H. 1994 *Nonlinear Dynamics and Chaos*. Perseus Books.

TAYLOR, G. K., NUDDS, R. L. & THOMAS, A. L. R. 2003 Flying and swimming animals cruise at a Strouhal number tuned for high power efficiency. *Nature* **425**, 707–711.

TRIANTAFYLLOU, G. S., TRIANTAFYLLOU, M. S. & GROSENBAUGH, M. A. 1993 Optimal thrust development in oscillating foils with application to fish propulsion. *J. Fluids Struct.* **7** (2), 205–224.

TRIANTAFYLLOU, M. S., TRIANTAFYLLOU, G. S. & GOPALKRISHNAN, R. 1991 Wake mechanics for thrust generation in oscillating foils. *Phys. Fluids* A **3** (12), 2835–2837.

TRIANTAFYLLOU, M. S., TRIANTAFYLLOU, G. S. & YUE, D. K. P. 2000 Hydrodynamics of fishlike swimming. *Annu. Rev. Fluid Mech.* **32** (1), 33–53.

VANDENBERGHE, N., ZHANG, J. & CHILDRESS, S. 2004 Symmetry breaking leads to forward flapping flight. *J. Fluid Mech.* **506**, 147–155.

WU, T. Y.-T. 1961 Swimming of a waving plate. *J. Fluid Mech.* **10** (03), 321–344.

https://doi.org/10.1017/jfm.2014.272 Published online by Cambridge University Press